Journal of Manufacturing Processes 57 (2020) 48–60

Contents lists available at ScienceDirect

Journal of Manufacturing Processes

journal homepage: www.elsevier.com/locate/manpro

The influence of processing parameters on piezoelectric and dielectric properties of dome-shaped composite PZT-epoxy actuators

W. Du[a], J. Hoyt[b], N. Williams[c], K.A. Cook-Chennault[d,e,f,*]

[a] Insight Data Science, Fellowship Program, San Francisco, California, 94107, United States
[b] University of Minnesota, Mechanical Engineering, 111 Church St SE, Minneapolis, MN 55455, United States
[c] Pratt and Whitney, Systems Engineering, 400 Main St., East Hartford, Connecticut, 06118, United States
[d] Mechanical and Aerospace Engineering Department, 98 Brett Road, Rutgers, The State University of New Kersey, 08854-8058, United States
[e] Biomedical Engineering Department, 599 Taylor Rd., Rutgers, The State University of New Jersey, Piscataway, NJ 08854-8058, United States
[f] Department of Educational Psychology, Rutgers, The State University of New Jersey, Piscataway, NJ 08854-8058, United States

ARTICLE INFO

Keywords:
Piezoelectric composite
Actuator
Strain coefficient

ABSTRACT

Thick film dome-shaped composite PZT-epoxy structures have been fabricated using a modified sol gel and spin coating technique. Processing parameters and polarization technique (Corona versus contact polarization) have been studied to elucidate their influence on piezoelectric and dielectric properties. The volume fraction of PZT was varied from 0.0 to 0.7 and the highest values for the longitudinal piezoelectric coefficient, effective dielectric constant (@1kHz) and dielectric loss (@1kHz), were 11.1 pC/N, 28.7 and 0.004 respectively for the PZT volume fraction equal to 0.7. The piezoelectric strain coefficient for this dome structure was 7 times higher than previously reported values for a composite PZT-epoxy dome structure of similar structure and composition. The sample morphology was examined with the aid of scanning electron microscopy (SEM) images. The piezoelectric strain coefficients, capacitance, and effective dielectric constant increased with increasing PZT volume fraction, in addition to the surface roughness. Samples that were Corona poled facilitated higher polarization voltages (45 kV/mm and 70 kV/mm) and resulted in higher values of piezoelectric strain coefficients. Investigation of composite structures such as these will advance the development of curved and hemispherical piezoelectric actuators with enhanced displacement and mechanical properties.

Introduction

Piezoelectric ceramics are widely employed as sensors and actuators because of their ideal electromechanical properties. Ceramic piezoelectric actuators are typically simple in structure and highly reliable [1]; render large actuation forces and rapid response times, and consume minimal power during operation [2]. Despite these advantages, piezoelectric ceramics are brittle in nature, which limits their operational strains [3], operational loading frequency, cycle life and compatibility to applications requiring complex shapes. These poor mechanical properties limit their effective application to devices such as; hydrophones [4,5], static and vibration based energy harvesting devices [6,7], surgical tactile sensors [2,8,9], biomedical scaffolds [10,11] and synthetic jet actuators [12]. Piezoelectric polymers, such as polyvinylidene fluoride (PVDF) are flexible, lightweight and have low acoustic and mechanical impedance, but suffer from low piezoelectric properties (d_{31} ~ 6-28 pC/N [13,14]). Composite piezoelectric materials leverage the ideal characteristics of disparate materials with dissimilar characteristics to tune the piezoelectric and dielectric properties towards increasing the design degrees of freedom for the application to advanced devices and systems.

Interest in dome and curved shaped piezoelectric devices has increased because these structures demonstrate higher deformation [15] and electromechanical conversion accuracy [16] in comparison to planar actuators [17–20]. A summary of work performed in dome-shaped piezoelectric devices is presented in Table 1. Dome-shaped piezoelectric actuators can also achieve large loading [21] and large electro-induced displacements [16] in comparison to planar bimorph and multilayer actuators. In this work, dome-shaped 0–3 connectivity piezoelectric composites comprised of lead zirconate-titanate (PZT) and epoxy were fabricated using a combination sol gel mix, spin coat, and cast method. The volume fraction of the PZT was varied from 0.1 to 0.7. The influences of the viscosity (composite mixture before the spin coat process) and polarization voltage, on the effective composite

* Corresponding author at: Mechanical and Aerospace Engineering Department, 98 Brett Road, Rutgers, The State University of New Kersey, 08854-8058, United States.
E-mail address: cookchen@soe.rutgers.edu (K.A. Cook-Chennault).

https://doi.org/10.1016/j.jmapro.2020.05.036
Received 8 November 2017; Received in revised form 4 May 2020; Accepted 21 May 2020
Available online 22 June 2020

Table 1
Overview of the state of the art in fabrication techniques and piezoelectric and displacement performance of dome-shaped piezoelectric devices.

Application - Processing & materials	ε / *tan* δ / k_{eff}	d_{33} /d_{31} *(pC/N)*	Loading Conditions	Poling Conditions
Unimorph(PZT-epoxy)/spin-coating[This work]	127@110 Hz	d_{33} = 11.106 d_{31} = 3.9	—	Corona poled a@ 45kv/mm (30 min)
Actuator - Unimorph(70% PZT)/spin-coating [22]	76.1 @110 Hz	d_{33} = 1.06 d_{31} = 0.74	Dome-down No-load	Contact poled 2.2kv/mm @ 75C for 15mins
Actuator - Single layer(0.04$Pb(Sb_{0.5}Nb_{0.5})O_3$–0.46$PbTiO_3$–0.5$PbZrO_3$)/PIM (powder injection mold) [17]	ε = 1450 / k_p = 0.7(material)	d_{33} = 550(material)d_{33} = 2.8 × 10^{-8} V/m*	–Dome-horizontal Load unclear	Contact poled 2.5kv/mm @ 150 °C in silicon oil for 40mins
PCA - Multi-layers (PZT, carbon-epoxy, glass-epoxy) Thermally induced [26]	—	d_{31} = d_{32}=-320 × 10^{-12} m/V (material)	Simple supported Dome-down Central line loading Fixed-free boundary Dome-down Central line loading	—
Actuator - Monolithic bilayer composite (piezo:0.65PMN-0.35 P T; electrostrictive: 0.9PMN-0.1 P T)/co-fire [27]	k_{33} = 20,000*(electrostrictive)*k_{33} = 630*(piezoelectric)*	d33 = 630(material, piezoelectric)	Unclamped Dome-down Tip-load	Contact poled 2.5kv/mm @ 150C in silicon oil for 10mins
Sensor - Multi-layers(PZT-5A, Aluminum, LaRC-SI adhesive film)/THUNDER [15]	80-95 nF @(10^{-3} Hz-100 Hz)	—	Fixed at four corners Dome-down No-load	Re-poling: 420v for 5mins
LIPCA-Multi-layer (PZT, Carbon/Epoxy, Glass /Epoxy)/ Thermally induced) [28]	—	d_{31} = -176 × 10^{-12} m/V(material)	Screw-fixed Dome-down Point load	—
Sensor - Single layer (PVDF-TrEE) Mold./Spin-coating [29]	—	Sensitivity 0.0108 V/N @5Hz	Clamped (fixed at circular edge) Dome-down Surface load	Contact poled 70kv/mm @90C for 30 min
Actuator - Double layer (PZT 53/47 doped with La^{3+}, Nb^{5+}, and PZT doped with Fe3 +, Ni^{2+})/conventional ceramic processing & pressing [30]	—	d_{31} = 108 —donor doped PZT d_{31} = 42 —acceptor doped PZT (material)	Dome-down No load	Contact poled 30 kV/mm @ 120 C in silicon oil.

piezoelectric and dielectric properties were investigated.

Less than a handful of groups have successfully fabricated dome shaped actuators using a combination sol gel engineered approach., which allows for tremendous flexibility in the processing of these types of structures. In our previous work [22], a sol-gel and spin-coating technique was used to fabricate 0–3 composite PZT-Epoxy dome-shape structures with filler volume fractions ranging from 10% to 70%. The values for piezoelectric strain coefficients, d_{33} and d_{31}, capacitance, *C,* and effective dielectric constant, ε, were 1.06 pC/N, 0.74 pC/N, 6.0 pF and 76.1 respectively at 70% volume fraction of PZT. It was determined that these devices had the potential to be applied as sensor/actuators, capacitors and low-power energy harvesting devices [22]. While the effective dielectric constant was comparable to the range of other works (32 to 71 [23,24]), the d_{33} values were low compared to other's (4pC/N to 24.8 pC/N [23–25]). The lower piezoelectric strain coefficient values were attributed to PZT agglomerations and air pockets within the matrix, which hindered the effectiveness of the polarization process. The purpose of this work is to investigate how processing techniques (polarization and spin coat deposition profile) influence the piezoelectric and dielectric materials properties.

Materials and methods

The results from optimized (final after all studies were completed) processing procedure are presented and compared to the results from our prior work [22]. In order to achieve the optimized processing steps described in this paper, a parametric study was performed to identify the influence of several processing parameters on the resulting piezoelectric and dielectric properties of the dome-shaped devices. The modified procedure for the fabrication of the piezoelectric dome structures is derived herein and is based on a Spin -Speed/Time Profile study and Deposition Technique Study. The dielectric constant, dissipation factor, resistivity, normalized impedance and phase of epoxy single-phase sample are measured over the frequency range of 2 kHz to 20 MHz. The longitudinal and transverse piezoelectric coefficients d_{33} and d_{31} were measured along with the capacitance to examine the relationship between PZT volume fraction and device performance.

This section is divided into four parts: Section 2.1: Materials, Section 2.2: Experimental Methodology, Section 2.3: Piezoelectric and Dielectric Characterization. In Session 2.1 an overview of the materials used for sample preparation is provided. In Section 2.2, overviews of the original and modified fabrication methods are presented, and in Section 2.3, the piezoelectric and dielectric characterization process is described.

Materials

The materials used in the previous work [31] and this work were maintained. In Table 2, the physical, dielectric and piezoelectric properties of the lead zirconate titanate ($Pb(Zr_xTi_{(1-x)})O_3$ – 855, Navy VI) and the two-part epoxy - DGEBA, EpofixTM Cold-setting embedding resin (purchased from APC International and Electron Microscopy Sciences, respectively) are detailed. An overview of the fabrication process from the previous work [31] is presented in Fig. 1. The values for the PZT are for bulk PZT as published by APC International. The values for the DEGBA were determined from an epoxy dome structure that was

Table 2
Physical, dielectric and piezoelectric properties of the materials used in the fabrication of piezoelectric dome shaped structures.

Property	PZT 855 [31] (Navy VI)	DEGBA
Relative dielectric constant, ε_r	3300	3.7-3.9
Dielectric dissipation, *tanδ*	≤ 2.50%	~0.002-0.004
Yong's Modulus, Y_{11}^E/ Y_{33}^E	5.9/5.1	2.21 ~ 2.7 [32]

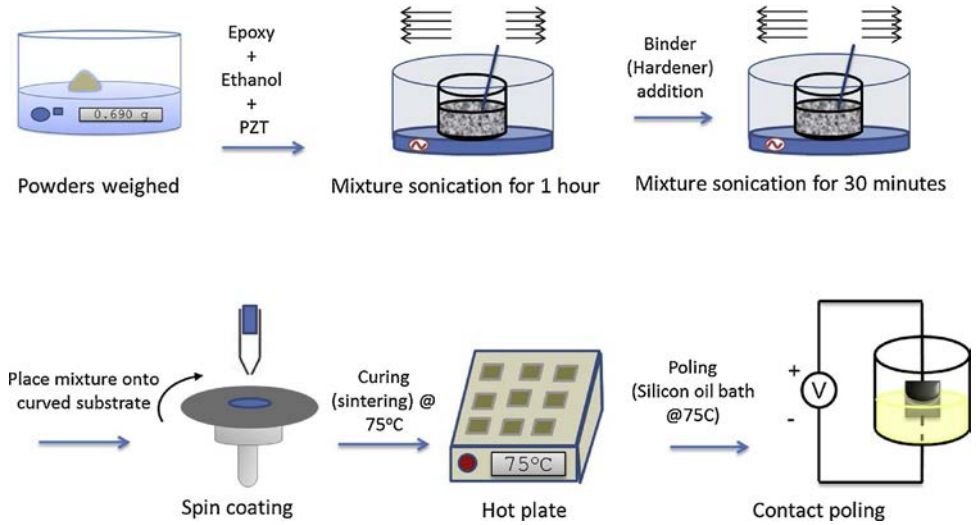

Fig. 1. Overview of the original method used from our previous work [22].

fabricated using the same steps as defined herein with 0% PZT.

In this paper, several modifications to the previous fabrication process were performed: 1) the addition of a desiccation step to eliminate air bubbles; 2) a modified spin coat deposition process based on observations from the study described in Section 2.2.1: Spin Coat Deposition Speed Study and Time Profile Study and Section 2.2.2: Sol Gel Layering Study; 3) maintenance of the sol gel viscosity to be within a range of 150–200 mPa s; and 4) the implementation of a Corona polarization process instead of the Contact Parallel Plate polarization process. The new fabrication procedure used for this paper is depicted in Fig. 2.

Methods

An overview of the fabrication methodology that was used for this work is provided in Fig. 2. The volume fraction of PZT was varied from 0.0 to 0.7. First, the PZT powder was ball milled for 24 h, where the mean diameter of the PZT after the ball mill step was observed to be ~0.97 microns. Next, adequate amounts of the PZT and the epoxy were weighed and mixed with ethanol (15 ml) by hand. The mixture was sonicated for 2 h, desiccated for 4 h, and then sonicated for an additional hour. Samples that had initial viscosity values less than 150mPas were subjected to additional sonication until the final viscosity was within the range of 150 to 200 mPas @100rpm. The resulting mixture was spin coated onto a dome shaped metal substrate. The substrate was stainless steel, Type 304, (Alfa Aesar, Ward Hill, MA, USA). The dome shaped stainless steel substrate was made by pressing the stainless-steel substrate in a mold at a pressure of 500 psi for 15 min at room temperature.

The dimensions for the dome structure are provided in Fig. 3. Once deposited, the dome shaped films were cured on a hot plate at 75 °C for 8 h.

The piezoelectric dome structures were heated using a hot plate for 10 min at 75 °C prior to corona polarization. Samples that comprising 10%–70% volume fraction of PZT were polarized at 45 kV/mm at a temperature of 75 °C in air for 30 min. The temperature of 75 °C was selected to obtain optimal cure quality and polarization characteristics. In particular, the curing agent used for the diglycidyl ether bisphenol A (DEGBA) liquid formulation achieves rapid reactivity above 70 °C, where it has been found with the aid of Differential Scanning

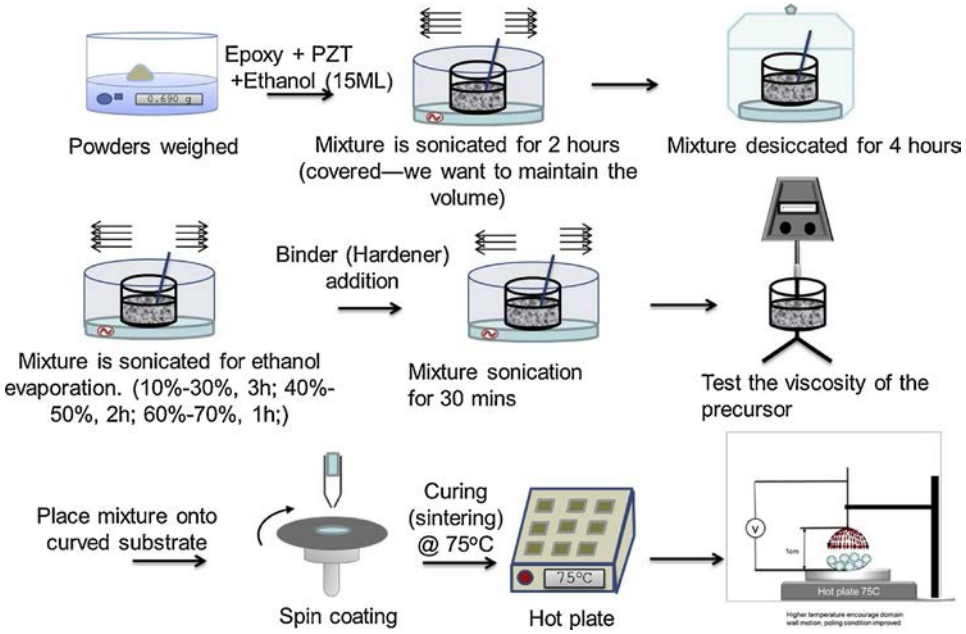

Fig. 2. Overview of the method of fabrication used for this work. Appropriate amounts of PZT, DEGBA and ethanol were weighed and then mixed and sonicated for 2 h. The mixture was subsequently dessicated for 4 h and sonicated for an additional hour. The binder was then added to the mixture and sonicated again. The final mixture was spined coated onto the dome-shaped stainless steel substrate and cured at 75 °C. Samples were corona polarized.

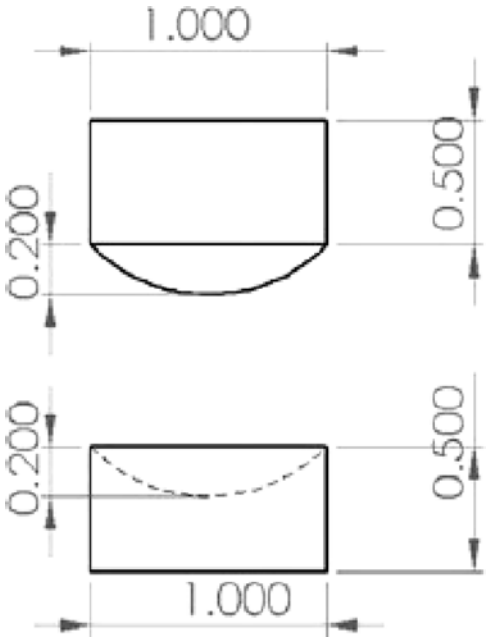

Fig. 3. The dimensions for the dome shape mold.

Calorimetry (DSC) analysis [33,34] that beyond this temperature there is an exothermic peak observed prior to an endothermic trough, which indicates the rapid crystallization of the DEGBA. The crystallization process of DEGBA is both quick and energetic, which allows for a quick return to a solid *steady-state condition.* However, the inclusion of a fillers increases the energy barrier during the cure process. This insight was coupled with the fact that the effectiveness of the polarization technique is dependent upon domain wall motion, which can be pinned by grain boundaries which develop electric fields due to crystallographic mismatches [35] that are enhanced at escalated reaction rates and subsequent solidification of the epoxy at elevated temperatures. Another set of samples (0.10, 0.20 and 0.30 vol fractions of PZT) were poled at 70 kV/mm at 75 °C for 30 min. The latter set of samples could be poled at a higher poling voltage due to the smaller volume fractions of PZT, while the former samples could not be polarized at the higher voltage. No top electrodes were used during the corona polarization process. The samples were wrapped in aluminum foil (to remove residual charges) and set aside for 24 h after the polarization process.

The film thickness of the samples was measured using mechanical calipers at 5 locations on the dome structure. These recorded thickness values were averaged, and these thicknesses were validated with the aid of SEM micrographs of the cross section of selected samples.

Two dependent studies were performed to determine the optimized deposition speed and time profile and deposition viscosity and layering for the dome-shaped structures. The two studies, speed/time and deposition layer were decoupled to independently understand the processing influence of sample performance. These two studies are described in Sections 2.2.1 and 2.2.2.

Spin coat deposition speed and time profile study

The spin coat speed and time increment studies were performed to ascertain the ideal characteristics for the spin coat speed and deposition step time for the fabrication procedure described in Fig. 2. An overview of the spin coat speed/time interval profiles studied are provided in Fig. 4. This study was done on samples with 0.50 vol fraction of PZT, where the viscosity of the sol gel was maintained at ~164.5 mPas @ 100 rpm. The amount of sol gel and *total* spin coat time was maintained at 2 mL and 220 s, respectively.

Sol gel deposition layer study

A Deposition Layer Study was performed because at PZT volume fractions less than and equal to 0.40, no piezoelectric strain coefficients were detected for samples that were subjected to the polarization process at 45 kV/mm and with sol viscosities between 150–200 mPa s. Hence, this study was conducted on samples where the volume fraction of PZT was a minimum of 0.40. The influences of the number of deposition layers, time interval between layer deposition and sol gel viscosity were examined.

An overview of the Deposition Layer Study is provided in Fig. 5. The steps before deposition were kept the same as those described in Fig. 2. For each sample fabricated, the amount of sol gel was maintained at 2 ml. The samples were fabricated at viscosities that were equal to 150, 248.7 and 299 mPas (the spin coat and deposition equipment was operated at 100 rpm). The films were deposited in one, two or three layers as shown in Fig. 5. The total amount of sol gel was maintained for each process and the same speed/interval profile was maintained for each layer deposition step. The datum sample included one deposition layer, where the measured viscosity prior to the application of the single layer was 150mPas.

Material characterization

In this work, the mechanisms that influence the piezoelectric and dielectric properties of composites are investigated as a function of the volume fraction of PZT with the aim of understanding the influence of fabrication technique on the aforementioned properties. The films were characterized in terms of their dielectric spectra, piezoelectric strain coefficients, dielectric loss (tan δ), impedance spectra and viscosity. The dynamic viscosity of the mixture was then measured using a Brookfield DV-E viscosity meter. The piezoelectric strain coefficients, d_{33} and d_{31} were measured at the frequency of 110 Hz using the PiezoMeter PM300. Frequency dependent capacitance, dielectric loss, resistance, conductance, impedance and phase spectra were measured with an impedance analyzer, HP 4194A Impedance Analyzer. The measured values were used to calculate the dielectric constant, resistivity and normalized impedance. The impedance was normalized with the area and thickness. The piezoelectric strain coefficients and the capacitance were initially measured without a top electrode. Then, electrically conductive silver paste was added to some samples for the top electrode, and the d_{33} values were recorded again and compared to the values where no top electrode was used. The dielectric impedance, phase angle, capacitance and dielectric loss ($tan\ \delta$) were measured as a function of frequency (2 kHz to 20 MHz) on samples that used aluminum tape as the top electrode. Ultimately, the aluminum tape was used instead of silver paste because the paste caused some samples to short circuit. The aluminum tape electrode was triangular in shape with an average area equal to 18.5 mm^2. The dielectric constant was calculated using Eq. 1. In Eq. 1, $\boldsymbol{\varepsilon_r}$ is the relative dielectric constant, $\boldsymbol{\varepsilon_0}$ is dielectric constant of a vacuum ($\boldsymbol{\varepsilon_0 \approx 8.854 \times 10^{-12} F \cdot m^{-1}}$), C is capacitance, A is area; d is the thickness of the piezoelectric composite layer.

$$\varepsilon_r = \frac{C \cdot d}{A \cdot \varepsilon_0} \tag{1}$$

The dielectric constants that were calculated from the measured values and were compared to an analytical model proposed by Furukawa [36], expressed in Eq. 2. In Eq. 2, ε, ε_1, ε_2 and $\varnothing$, are the effective dielectric constant of the composite, the dielectric constant of the epoxy matrix, the dielectric constant of the PZT, and the volume fraction of the inclusions, respectively.

$$\varepsilon = \frac{2\varepsilon_1 + \varepsilon_2 - 2\varnothing(\varepsilon_1 - \varepsilon_2)}{2\varepsilon_1 + \varepsilon_2 + \varnothing(\varepsilon_1 - \varepsilon_2)}\varepsilon_1 \tag{2}$$

The piezoelectric strain coefficient was compared to the coefficients predicted by Furukawa's [37] analytical expressed in Eq. 3. In Eq. 3, d_{33} is the piezoelectric strain coefficient, $L_s = \frac{1}{\varnothing}\frac{c_1 - c}{c_1 - c_2}$ and $L_E = \frac{1}{\varnothing}\frac{\varepsilon_1 - \varepsilon}{\varepsilon_1 - \varepsilon_2}$. In Eq. 3, c, c_1 and c_2 are the Young's Moduli of the composite, matrix and

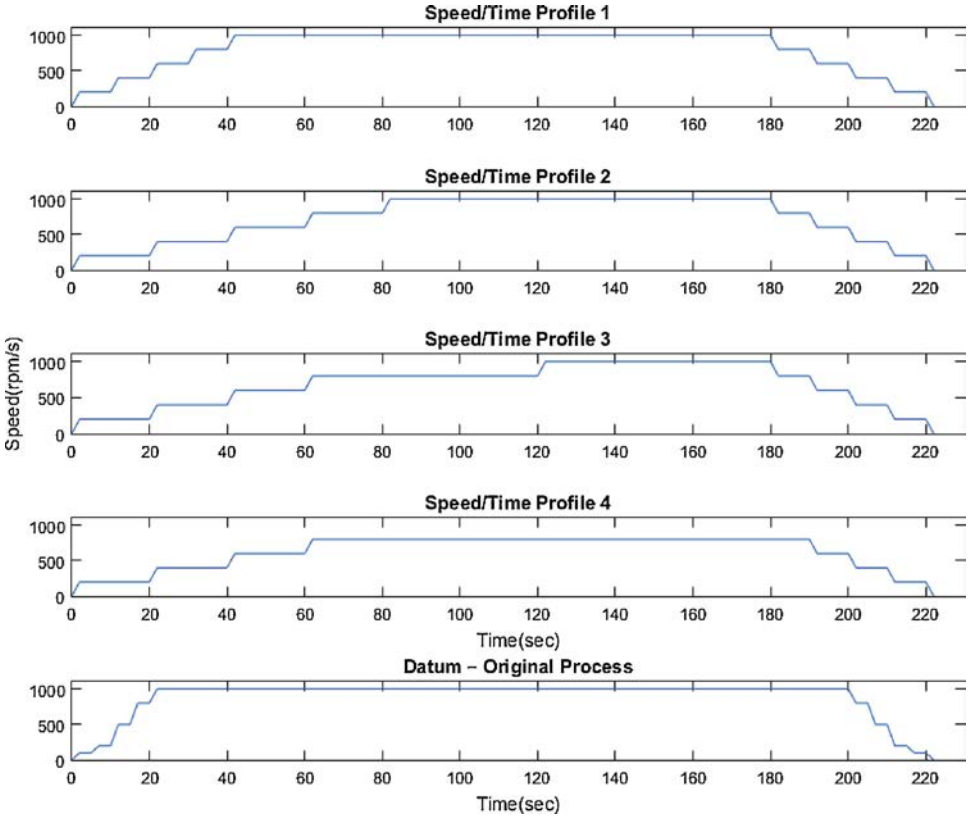

Fig. 4. Speed/Time profiles studied. The datum process has step intervals of 100, 200, 500 and 800 rpm for 5 s each for spin initiation/conclusion, and the middle process was held at 1000 rpm for 3 min.. Profile 1 includes step intervals of 200, 400, 600, 800 and 1000 rpm for 10 s each during the ascension and descension, while a speed of 1000 rpm is held for 140 s. Profile 2 uses the same ascension and descension steps as Profile 1, but the time held for 200, 400, 600, 800 rpm are 20 s each, while the hold time at 1000 rpm is 100 s. Profile 3 is built on Profile 2 by extending the hold time at 800 rpm to 1 min, and reducing the hold time for 1000 rpm to 1 min. Profile 4 is built on Profile 2 by eliminating the speed step at 1000 rpm, the top speed in this profile is 800 rpm, and is hold for 130 s.

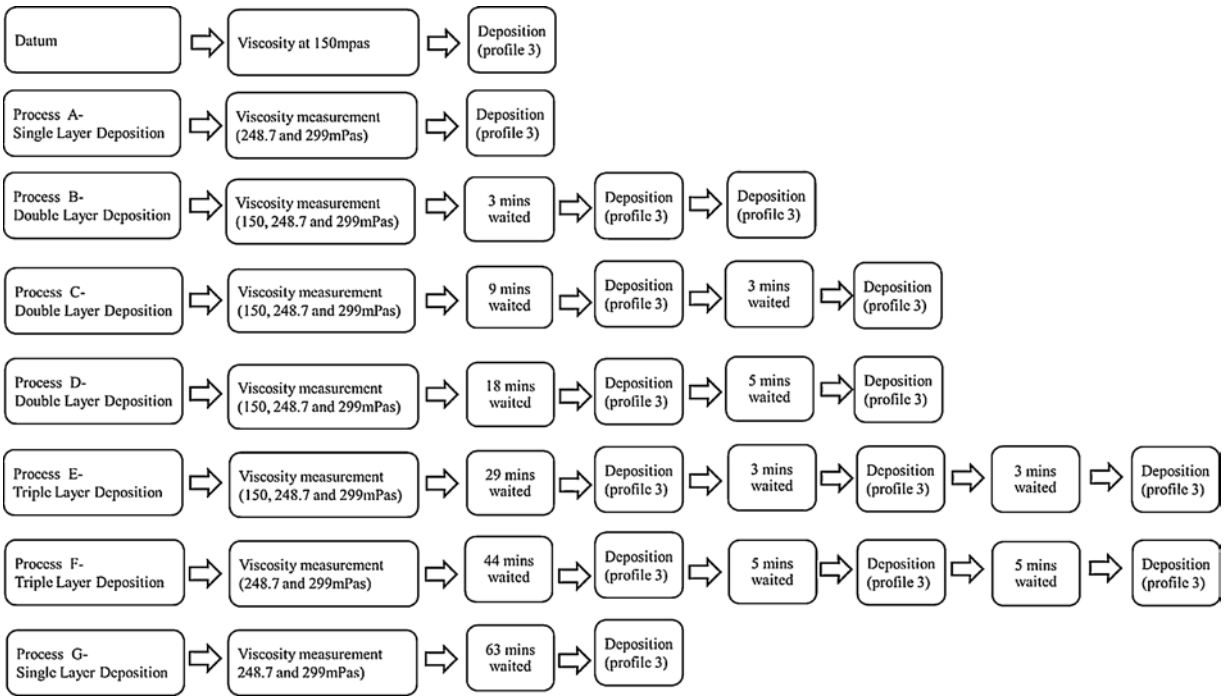

Fig. 5. Overview of the deposition layer and sol viscosity study. All of the processes described in this figure incorporated Speed/Interval Profile 3 for the "Deposition" step. Three viscosity settings were used: 150 mPas, 248.7 mPas and 299 mPas.

PZT inclusions, respectively and the subscripts 1 and 2, denote the matrix and PZT inclusions respectively.

$$d_{33} = \frac{1}{c} \bullet \varnothing L_s L_E d_2 c_2 \tag{3}$$

Process A included two data sets, where the first set of samples was fabricated with one deposition layer at a measured viscosity equal to 248.7mPas and the second data set had a viscosity of 299mPas. Processes B, C and D incorporated two layers of deposition. Three sets of samples were prepared using Process B where the measured viscosities for each data set were equal to 150, 248.7 and 299 mPas, respectively. The time interval between the deposition of the first and

second layers (for Process B) was three minutes. Similarly, three sets of samples were prepared using Processes C and D, and the viscosities were measured to be equal to 150, 248.7 and 299 mPas, respectively. The time intervals between the deposition of the first and second layers were 9 and 3 min for Process C, and 18 and 5 min for Process D, respectively. Three layers of deposition were used for Processes E and F, and three sets of samples were prepared at viscosity values equal to 150, 248.7 and 299 mPas, respectively.

The time increments between the deposition of the layers for Process E were equal to 29, 3 and 3 min, and equal to 44, 5 and 5 min, respectively for Process F. Process G was implemented for the fabrication of two data sets of samples at viscosities equal to 248.7 and 299 mPas, respectively. A single time interval of 63 min was taken prior to the deposition of the first and only layer.

The piezoelectric dome shaped composites underwent polarization following the process described in Fig. 2 after the layer(s) were deposited onto the stainless-steel substrates and pressed. The devices were Corona polarized at 45 kV/mm and were allowed to age one day before the measurement of the piezoelectric strain coefficients, thicknesses and dielectric properties.

The fractured surface morphology and Electron Dispersion Spectroscopy (EDS) of the samples were studied with using micrograph images obtained from a Scanning Electron Microscope (SEM) (FESEM ZEISS 982) to ascertain the distribution of the PZT filler in the matrix, PZT filler mean size, degree of separation of particles, particle morphology, composite porosity and agglomeration.3.

Results and Discussion

The results obtained in this work were compared to our previous work and analytical models at corresponding volume fractions. The piezoelectric coefficients with silver paste electrodes were compared to those without top electrodes, our previous work and an analytical model. Piezoelectric coefficients d33 and d31 were measured on samples polarized by 70 kV/mm and compared to samples poled 45kv/mm in this work, previous work and an analytical model. The surface morphology of samples was examined using a scanning electron microscope (SEM) and energy-dispersive X-ray spectroscopy (EDS).

Spin coat deposition speed and time profile study

The results from the spin coat speed and time interval studies are in Table 3. In Table 3, it is observed that the sample that was fabricated using Profile 1 had no piezoelectric response, which could be because the piezoelectric layer was so thin that there was not enough piezoelectric material in the layer to produce a readable piezoelectric response.

Samples fabricated using Profiles 2 and 3 demonstrated reasonable d_{33} values that were > 7 pC/N (the largest of the four profiles and datum). Samples fabricated using Profile 3 had a uniform thickness and highest value of d_{33} (7.52 pC/N).

Sol gel deposition layer study

The deposition study (over in Table 4) was done on 0.40 vol fraction of PZT. There were three starting viscosities, 150mPas, 248.7mPas and 299mPas respectively for this study, with 8 processes (A, B, C – G) including the datum study. As shown in Table 4, the sample fabricated with the datum process had no piezoelectric response, and neither do samples fabricated using process A, which had elevated viscosities in comparison to the datum. In the datum and Process A, samples that were thinnest had relatively low viscosity < 299mPas. The low volume fraction of PZT deposited on the substrate during the deposition process, could be the cause of negligible piezoelectric response. Moreover, poling voltage was calculated based on the thickness of piezoelectric layer, which meant that low corona poling voltage could also lead to insufficient polarization.

Processes B, C and D incorporated two deposition layers. Samples that utilized the viscosity less than 249 mPas described for Process B expressed no piezoelectricity. Samples that were layered with an initial viscosity of 299mPas (Process B and C) had d_{33} values > 4.3 pC/N, i.e. 4.32 and 5.6 pC/N for Process B and C, respectively. Samples that were fabricated using Process C were polarized at a voltage of 45 kV/mm. Samples that were fabricated using the same process, but with lower viscosity had no piezoelectric response. Samples that were fabricated using Process D (higher viscosities, i.e. 248.7mPas and 299mPas) presented higher piezoelectric values. These samples experienced longer wait times prior to deposition of layers as detailed in Table 4, which could have enabled higher amounts of PZT particles to be included within the samples thickness. Samples fabricated using Processes E and F incorporated three layers of deposition as shown in Table 4. All samples fabricated using Process E demonstrated d33 values regardless of the initial viscosity employed. However, these samples incorporated longer wait times, (29 min detailed in Fig. 5), prior to the deposition of electroactive layers. All of the samples fabricated using process F experienced dielectric break down during the poling process, though the initial viscosity was comparable to that used for Process E. The number of electroactive layers and presence of air gaps between layers resulting in contact resistance may have enhanced the probability of dielectric breakdown not evidenced in samples fabricated using Process B, C and D. All these studies show that consistent and fairly high piezoelectric coefficients could be achieved with samples of low volume fraction, i.e. 10–40% PZT however, multiple deposition layers at specific viscosities are required in order for a favorable thickness to be realized. Also, variation in layer thickness can be minimized when the deposition viscosity is increased to 300mPas-350mPas or when the viscosity is maintained in 150–300 mPa s and Profile E is employed.

Summary of optimized processing conditions

An overview of the data captured from samples where optimized processing conditions obtained from studies mentioned above are detailed in this section. Spin/Speed Profile 3 (detailed in Fig. 4) rendered the highest d33 values regardless of PZT vf and deposition layer process. Samples fabricated using corona polarization produced higher d_{33} coefficients than contact polarization.

PZT-epoxy dome – optimized fabrication method

In this section, a comprehensive summary of results from the optimization processes presented in Section 2 for PZT vfs ranging from 0.10

Table 3
Spin-Speed /Time Profile Study Results.

	piezoelectric layer thickness (mm)	Error(+)	Error(-)	Poling voltage (kV)	Poling electric field (kV/mm)	d_{33}(pC/N)	Error(+)	Error(-)	Dielectric constant	Error(+)	Error(-)
Profile (1)	0.105	0.005	0.007	4.7	45	−0.025	0.02	0.02	25.36	6.6	4.67
Profile (2)	0.141	0.004	0.002	6.3	45	7.26	0.29	0.26	45.08	6.57	3.79
Profile (3)	0.177	0.021	0.021	8.0	45	7.52	0.24	0.25	61.07	9.16	6.28
Profile (4)	0.241	0.037	0.042	10.8/7.8	45/32.5	4.27	0.36	0.17	101.44	2.24	1.89
Datum	0.089	0.06	0.06	4.1	45	0.02	0	0	20.06	8.23	7.2

Table 4
Sol Gel Deposition Study Results.

Profile	Viscosity (mPas)	d_{33} (pC/N)	Average capacitance (pF)	Piezoelectric layer thickness (mm)	Calculated dielectric constant	Corona poling electric field (kV/mm)
Datum/Normal	150	0.01	22.9	0.065	34.23953	45 kV/mm
Process A	248.7	0.01	21.7	0.087	43.42681	
	299.3	0.02	22.4	0.115	59.25498	
Process B	150	0.02	20.8	0.085	40.66879	
	248.7	0.02	20.8	0.127	60.76396	
	299.3	4.32	20.08	0.147	67.89848	
Process C	150	0.02	23.22	0.093	49.67343	
	248.7	0.01	22.3	0.113	57.96453	
	299.3	5.45	20.94	0.149	71.76983	
Process D	150	0.03	24	0.103	56.8627	
	248.7	5.78	19.9	0.175	64.5433	
	299.3	5.51	19.25	0.167	73.94796	
Process E	150	5.51	20.5	0.129	60.83066	
	248.7	5.74	18.43	0.173	73.35487	
	299.3	5.37	18.42	0.179	75.84407	
Process F	248.7	4.62	15.4	0.217	76.87045	Dielectric break down @45 kV/mm
	299.3	4.02	15.76	0.227	82.29265	
Process G	248.7	0.04	19.45	0.118	52.79352	45kv/mm
	299.3	4.34	19	0.143	62.49836	

to 0.70. Corona polarization at 45kv/mm was used and the viscosity of the sol gel prior to the deposition of the first layer was maintained between 150 to 250 mPas. Samples with vfs > 0.40 PZT were fabricated using Spin/Speed Profile 3 (Fig. 4) and datum process (Fig. 2), while samples with vfs < 0.40 PZT were fabricated using Spin/Speed Profile 3 (Fig. 4) and Process D (Fig. 5).

It was found that samples that were less than 0.50 vol fraction of PZT were ~39 μm thinner than the samples with higher PZT vfs, which may be due to the ability of more sol to adhere to the surface of more PZT particles of higher volume fractions and the faster cure rate observed for high volume fractions. In addition, at high vfs of PZT, i.e. 0.6 and 0.7, the agglomerated PZT filler decreased the mobility of other PZT particles due to particle collisions [38], where these collisions dominate the immobilization of particles instead of the shear stress provided by epoxy.

The d_{33} values for this work (with and without electrodes), from [22] and predicted by Furukawa's analytical model [36] are shown in Fig. 6. Similar to the trends observed by Furukawa et al. [36] and Seema et al. [39], the d_{33} values increase with the volume fractions of PZT. For example, B. Satish et al. [40] fabricated PZT-PVDF 0–3 composites and found that the piezoelectric coefficient expressed a positive correlation with the increasing volume fractions of PZT, which was also found by [22], where PZT bulk samples and thick films were fabricated and measured. The values they presented are comparable with our results which are 11.106 pC/N @70% volume fraction of PZT. However, some of our results are less than others (Satish et al. [40] reported d_{33} ~28 pC/N) because our matrix material in electrically inactive, while others integrated PVDF as a matrix material, which has piezoelectric proper ies. The d_{33} values from this work are one magnitude higher than the values obtained from previous work [22] for several reasons. First, the sonication time was increased, which resulted in better dispersion of PZT particles and the Corona polarization technique allowed to the use of higher polarization voltages, which improved the efficacy of the polarization process. Modification of the layering of electroactive films enabled better properties for lower volume fractions.

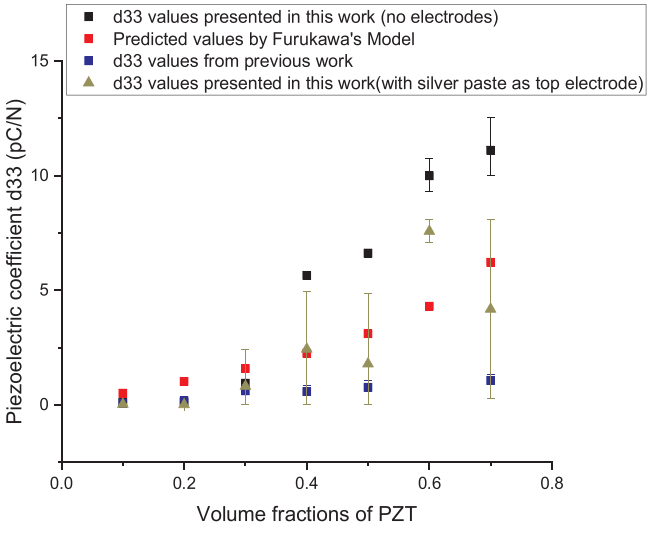

Fig. 6. Piezoelectric strain (d33) values of this work (without top electrode), this work (with silver paste as top electrodes), previous work, and predicted values by Furukawa are plotted.

The experimental values obtained in the present work agree with theoretical values (provided in Fig. 6). For higher volume fractions of PZT, the experimental values are higher than predicted values by Furukawa et al. [36,37], because Furukawa's model assumes a uniform distribution and perfectly spherical filler, however the PZT filler used varies from 1 to 10 μm with shapes varying from spherical to ellipsoid. At high volume fractions the PZT agglomeration occurs, which make the local electric fields around the filler higher than the theoretical values leading to higher piezoelectric responses. The transverse piezoelectric coefficients $-d_{31}$ values of this work and previous work are shown in Fig. 7. The values of our present work are comparable to others, e.g. Furukawa et al. [36,37], wherein they produced PZT-PVDF 0–3 composites with 0.21 vol fraction PZT that piezoelectric strain coefficients equal to 4 pC/N. The piezoelectric strain coefficients are also comparable to samples that were thicker in geometry and fabricated with PZT powder with larger mean diameter size such as [41] (d_{33} = 18 pC/N and 1 mm thickness, and 50% vf), [42](d_{33} = 13 pC/N, 13.8 pC/N, 14 pC/N for PZT/PVC, PZT/PVDF and PZT/PVDF samples respectively [42,43]. In addition, the piezoelectric strain values are higher than others of similar composition at comparable volume fractions [31,44]. These results indicate that piezoelectric strain coefficients are influenced by several factors: the enhanced polarization field achieved via the Corona technique versus contact method, 2) reduction in PZT agglomeration via processing technique; and 3) dome-shaped geometrical structure of the sample that allows for better actuation response for applied loading conditions.

Capacitance was measured at room temperature @110 Hz, and the

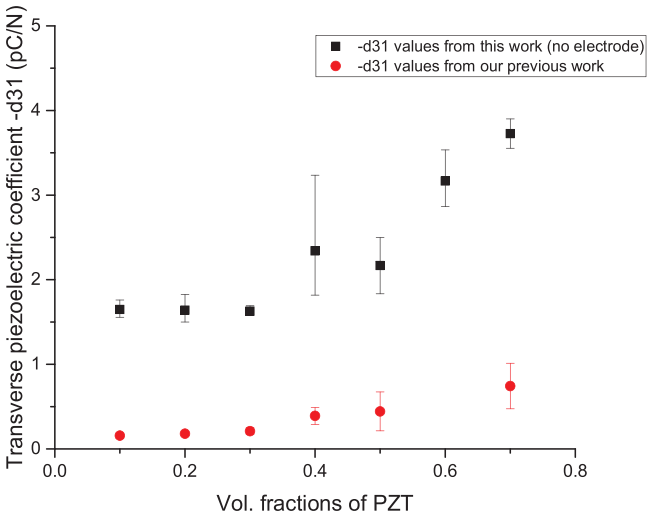

Fig. 7. Piezoelectric coefficient -d31 values of this work and previous work. The samples from previous work were contact poled, and the samples from this work were corona polarized at 45 kV/mm, with no electrode applied in both cases.

Table 5
Comparison of piezoelectric strain coefficients (0.7 PZT) corona and contact poled.

	Contact Poled 0.7 PZT	Corona Poled 0.7 PZT
Piezoelectric strain coefficient, d_{33}	1.18 pC/N	11.11 pC/N
Piezoelectric strain coefficient, d_{31}	0.75 pC/N	3.73 pC/N
Dielectric constant	76.10	53.87

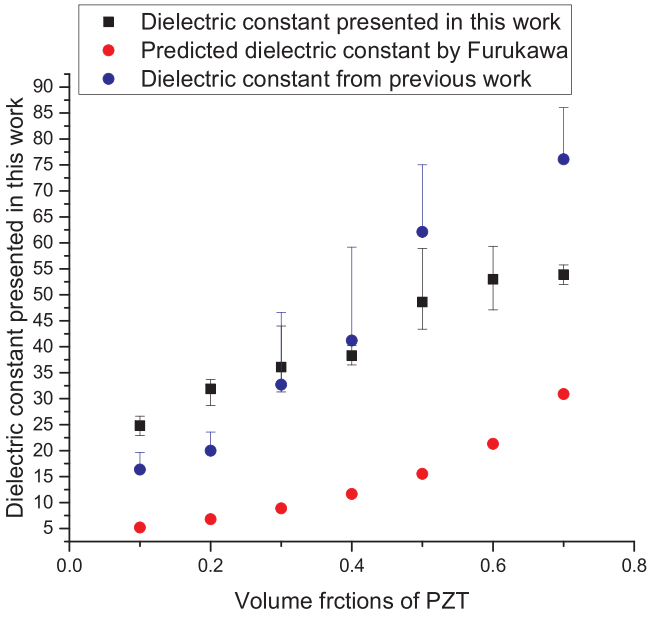

Fig. 8. Dielectric constant of present work, previous work and predicted values by Furukawa. No electrodes applied in both cases.

dielectric constant was calculated using Eq. 1. In both the previous work [22] and this work, the dielectric constants increased with the volume fractions of PZT. The dielectric constant of this work are slightly smaller than previous work [22] because of the reduction in agglomerated PZT and the associated surface charge and contact resistance, which promote higher capacitive storage. It is believed that ionic and electronic polarization mechanisms contributed to most to the higher dielectric constant values observed in this work. The agglomerations could be treated as effective larger particles, and the large particles could lead to higher dielectric constants as the interaction force between parties leads to the distortions toward more tetragonality [45]. As in Fig. 6, the experimental values and the predicted values have similar trends, and experimental values and predicted values are comparable. In Table 5, a comparison of our previous work[22] and this present work for 0.7 vf of PZT is presented Fig. 8.

In Fig. 9, the d33/d31 for samples polarized at 70kv/mm (which could only be achieved at lower PZT volume fractions less than 0.40) are higher than samples poled with 45kv/mm. The d_{33} captured from samples poled at 70kv/mm are more in agreement with the predicated values than samples poled at 45kv/mm shown in Fig. 6. Transverse piezoelectric strain, d_{31} values are similar regardless of polarization technique, but Corona poled samples have higher d_{31} values than contact polarized samples. These results indicate that the corona polarization technique is more effective than the contact polarization method for piezoelectric 0–3 composites, such as these. This can be seen by the enhanced values of dielectric constant, ε, and the strain coefficients d_{33} and d_{31} for all volume fractions. The increase in the strain coefficients is due to the increase in effectiveness of the polarization process. The dielectric constant, which is measured in the 33-direction is also enhanced due to the increase in the number of the dipoles aligned along the 33-direction.

In Fig. 10, the dielectric constants from our previous work and this present work are plotted as a function of the frequency range, dielectric constants increase as a function of vf of PZT. Space charge polarization is mostly responsible for the lower frequencies, while the values for the higher frequencies are most likely due to the effects of dipolar, ionic and electronic polarizations, since space charge polarizations do not present well at the higher frequencies. Within 1MHz ~ 10 MHz frequency range, the dielectric constant is mostly the result of ionic and electronic mechanisms since both the space charge polarization and dipolar polarization could not follow the change of the external electric fields. The increasing dielectric constant with frequency above 10 MHz could be from the epoxy phase. The dielectric constant of present work is slightly smaller (43.7–68.1) than others of similar composition (PZT/PVC, PZT/PVDF, PZT/epoxy) [31,42,43,46]; this could also be because of the reduction of the sample thickness, as there was less dielectric material and smaller mean diameters of the PZT embedded in the matrix material.

The dissipation factors are depicted in Fig. 11, and increase with the vf of PZT. The dissipation factor of PZT (~2.5%) is higher than the epoxy matrix (0.002 ~ 0.004). The spectrums show a substantial increase with the frequency, as epoxy's dissipation factor is relatively stable, so the increase is due to PZT. The dissipation factors of this work are smaller than previous work[22], due to the reduction of trapped air in the samples and better distribution of PZT. Space charge polarization occurs on the interface between the air pockets and composites material. This polarization induces the formation of two charge layers at the interfaces, however, this form of polarization cannot always be achieved at higher frequencies, in which case, the energy is dissipated as heat, resulting in higher dissipation factors.

In Fig. 12, the impedance in our present and previous works decreases with the vf of PZT, while the impedance of the present work are significantly lower than our previous work, due to the reduction in agglomerated PZT particles and reduced air gaps. Under the influence of an electric field the dissolved free ions tend to move towards the electrode/epoxy interface, leading to the development of ionic double layers in such regions, which is called space charge polarization [47]. This phenomenon could largely affect the measured resistant spectra.

In Fig. 13, in both our previous and present work, the phase angles increase with frequency, which is due to the response of the material, which is different than a pure capacitive circuit, where the phase of the voltage is 90° behind the alternating current. The increase in phase

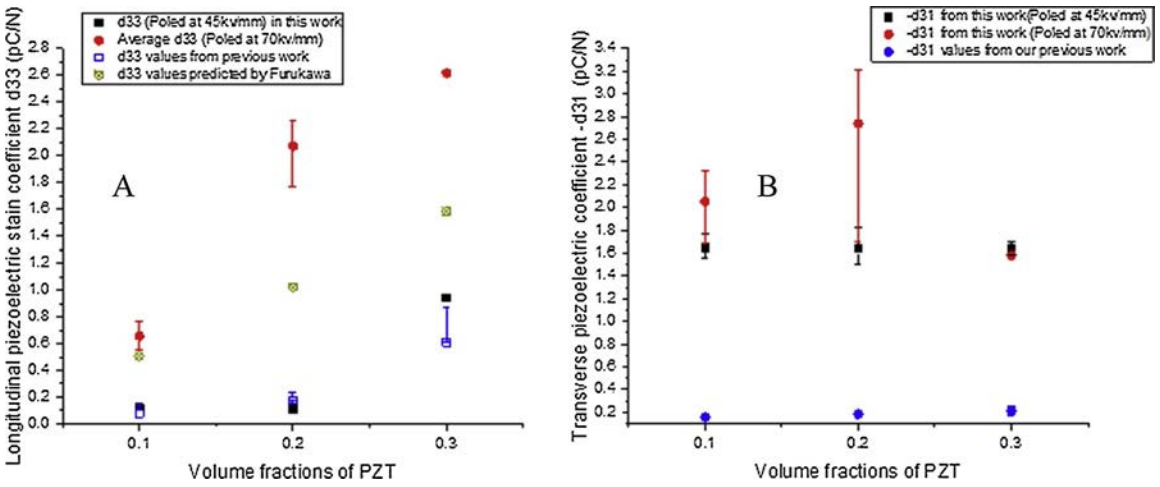

Fig. 9. A) Longitudinal piezoelectric coefficient d33 of previous work, this work (corona poled at 70kv/mm), this work (corona poled at 45kv/mm) and predicted values from Furukawa (only for d33) and B) Transverse piezoelectric coefficient d31 of previous work, this work (corona poled at 70kv/mm), this work (corona poled at 45kv/mm) and predicted values from Furukawa (only for d33).

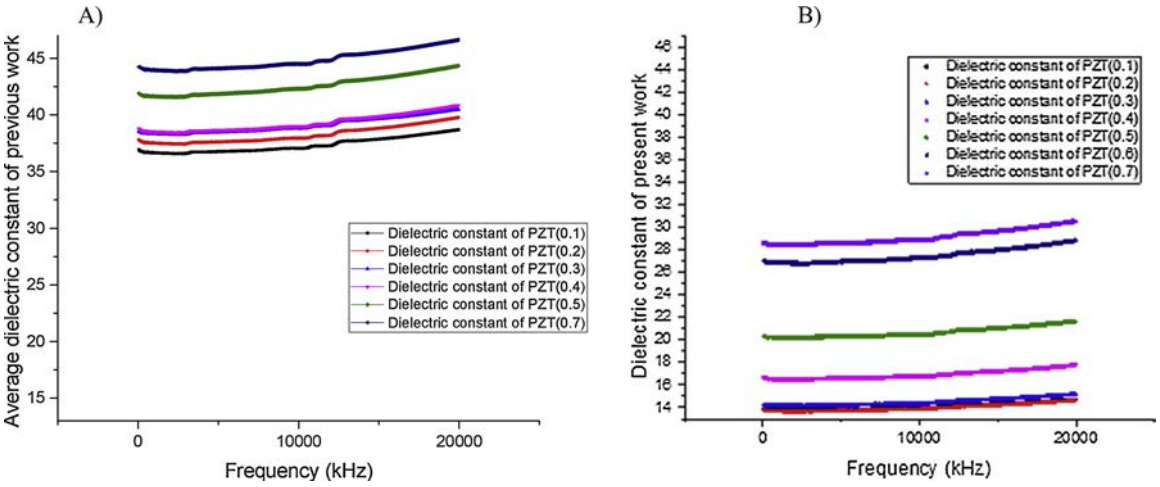

Fig. 10. The dielectric spectroscopy (2 kHz-20 MHz) of A) previous work and B) this work, both sets of spectra were obtained with small triangular aluminum tape as top electrode in both cases.

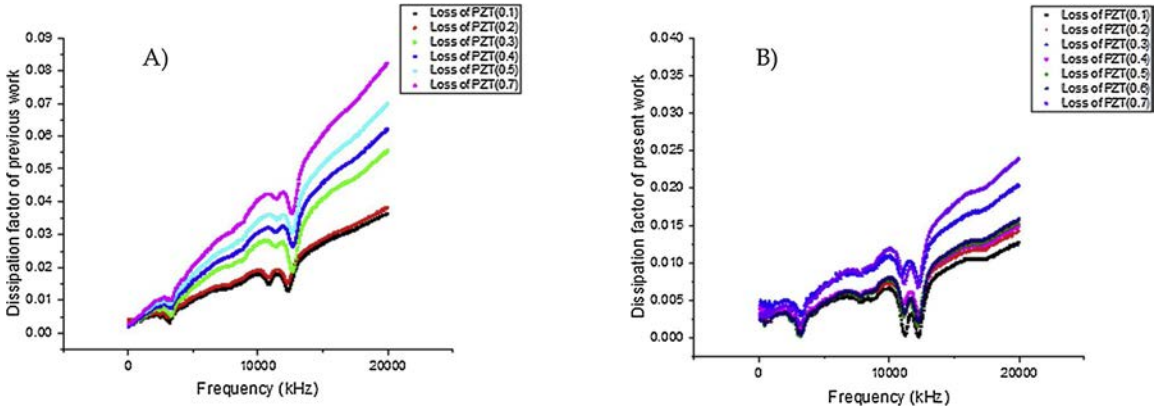

Fig. 11. Dissipation factor verse frequency (2 kHz-20 MHz) of A) previous work and B) this work, the spectrums were obtained with small triangular aluminum tape as top electrode for both cases.

angle with frequency is because the material is less dielectric at higher frequencies. The phase angle also increases as the volume fraction of PZT increases. In the present work, the phase angles for each volume fraction are lower than the values from our previous work, which could indicate that the updated method of fabrication leads to samples with better capacitive properties.

Surface morphology and PZT dispersion within the matrix

The mean and median diameter of PZT particles and clusters were characterized via SEM micrograph images and analysis software was

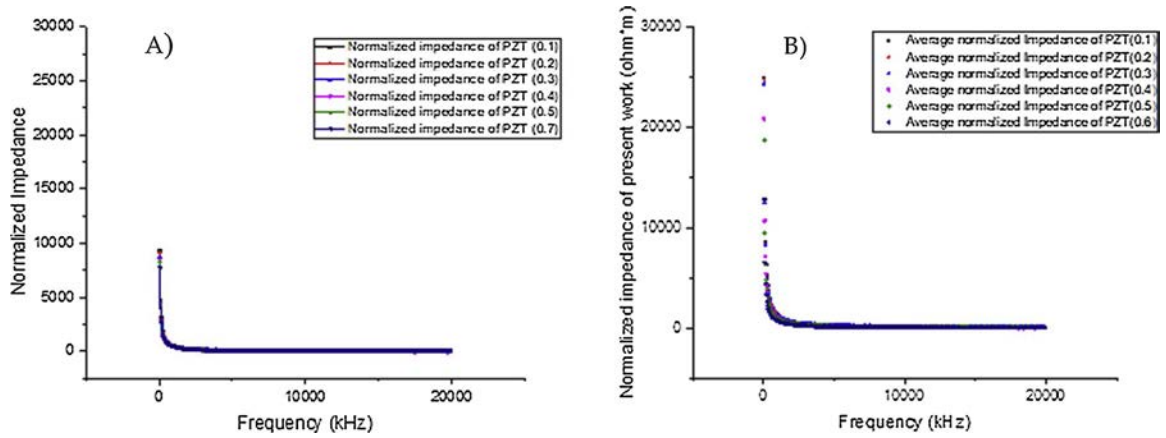

Fig. 12. Normalized impedance verse frequency (2 kHz-20 MHz) of A) previous work and B) this work, the spectrums were obtained with small triangular aluminum tape as top electrode for both cases.

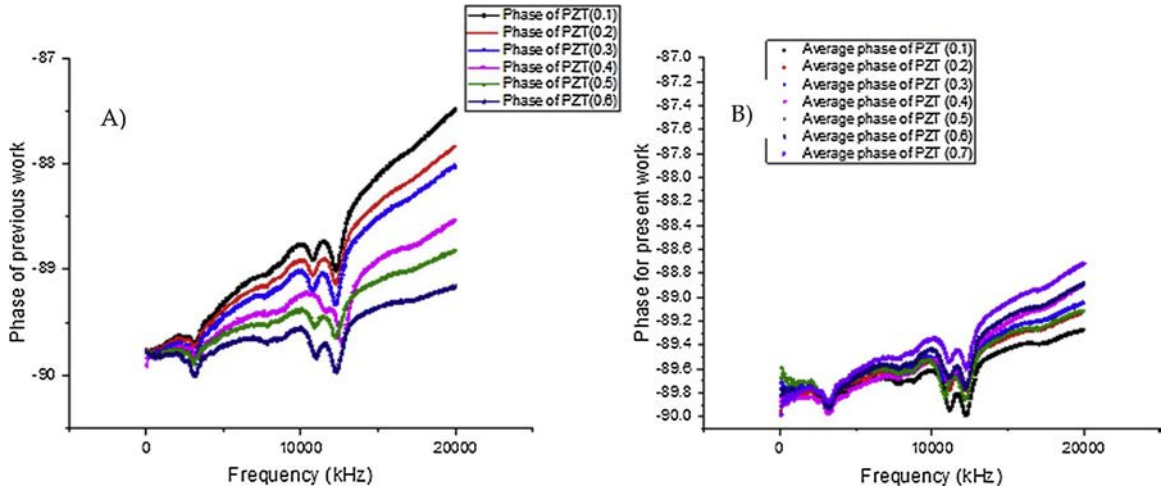

Fig. 13. Phase verse frequency (2 kHz-20 MHz) of previous work and this work, the spectrums were obtained with small triangular aluminum tape as top electrode for both cases.

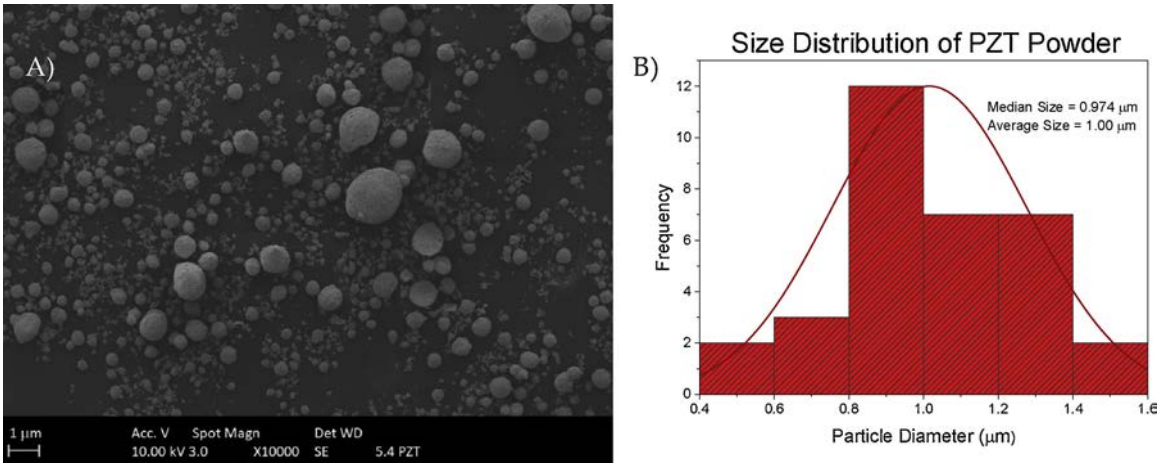

Fig. 14. A) SEM micrograph images of pristine PZT particles/clusters and B) particle distributions used to determine the mean (average) and median particle/cluster sizes, which were 1.00 and 0.974 µm respectively.

used to perform particle distribution analysis, as shown in Fig. 14. Fig. 15 depict the surface morphology of 50%PZT and 60%PZT composites. The distribution plot shown in Fig. 14 indicates that the average particle size and median PZT particle diameter are 0.974 and 1.00 µm, respectively. The surface morphology of the domed-shaped PZT-epoxy composite are observed with the aid of SEM images shown in Fig. 15 for samples of 50% and 60% volume fraction of PZT. These images indicate similar PZT cluster sizes with some aggregated PZT clusters in Fig. 14. There are small porous regions shown for the 50% PZT volume fraction (Fig. 15 A)). On the otherhand, the samples with

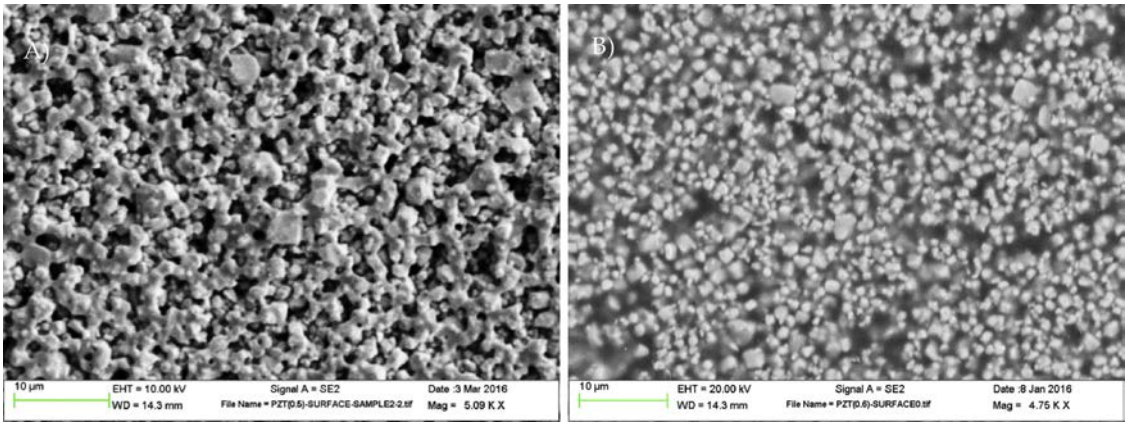

Fig. 15. SEM micrographs of A) PZT (vf = 0.5) and B) PZT (vf = 0.6) embedded within an epoxy matrix in the dome shaped structure.

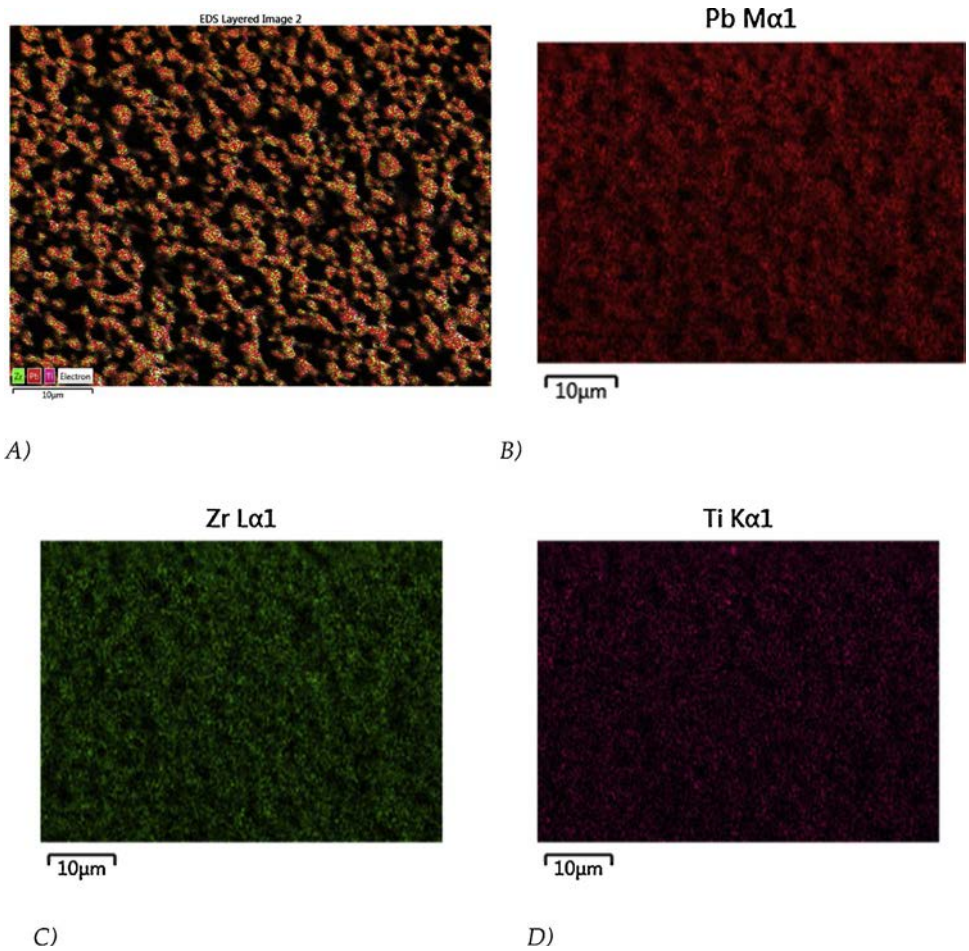

Fig. 16. EDS images of PZT(0.5)-Epoxy 0–3 dome shape structure. A) SEM images with distribution of Pt, Zr and Ti. B) Distribution of Pb. C) Distribution of Zr. D distribution of Ti.

the higher volume fraction (v_f = 60%)of PZT is denser with less porosity. EDS micrograph images were taken for samples comprising 50% and 6-% volume fraction of PZT and are depcited in Figs. 16 and 17, respectively. These images illustrate the distribution of PZT in the epoxy matrix. From the images in Fig. 17, there PZT apppears to be well-distributed throughout the matrix, however, the porosity of the sample is higher than that of the 60% volume fraction samples. Reduction in pores shown in Fig. 17, could lead to more effective polarization. The distribution of particles and sample porpsity is better than those of previous work [31], and enhancement of polarization due to reduced porosity and better PZT distribution are evidenced by higher values in piezoelectric strain coefficiencts than [31].

Conclusions

Novel PZT-epoxy composite thick films were fabricated using an optimized combination solvent and spin coat deposition technique for the synthesis of dome-shapes actuators. Parametric studies were performed to achieve the optimal fabrication procedure according to volume fraction of PZT. The surface and morphology were examined via

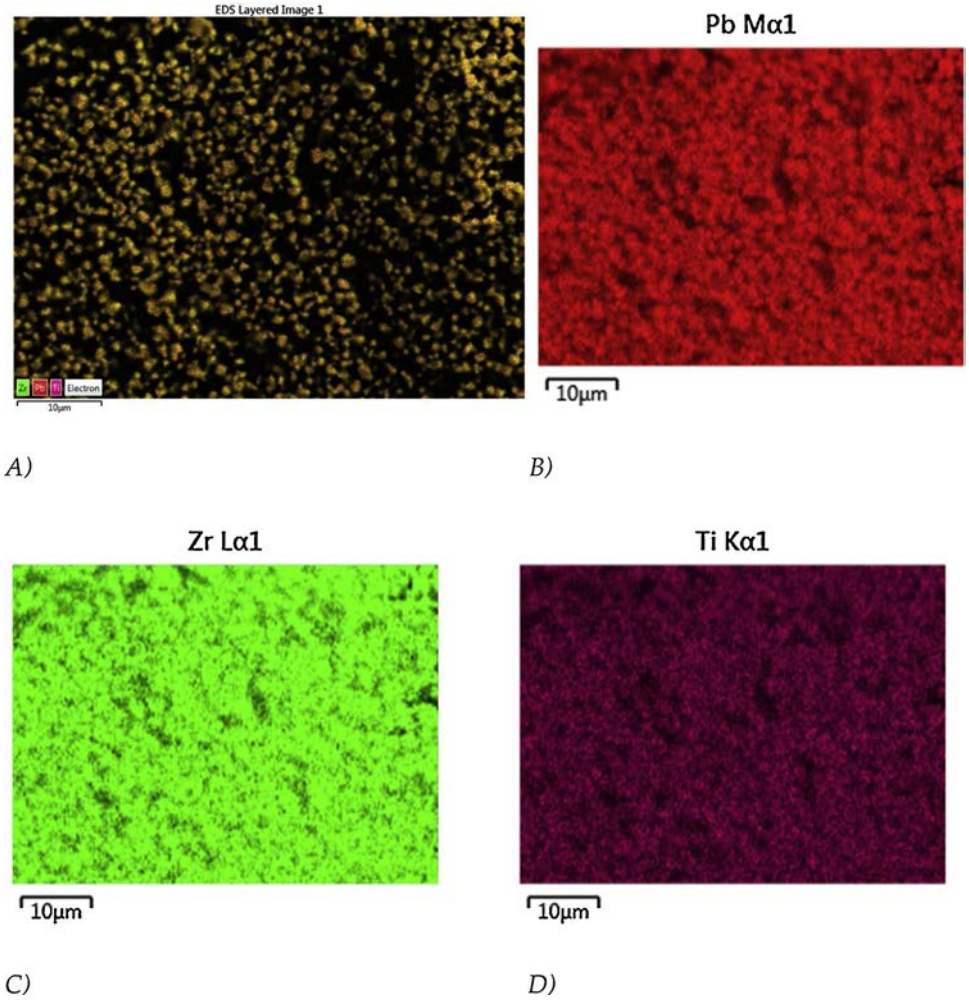

Fig. 17. EDS images of PZT (0.6)-Epoxy 0–3 dome shape structure. A) SEM images with distribution of Pt, Zr and Ti. B) Distribution of Pb. C) Distribution of Zr. D distribution of Ti.

SEM and EDS. The piezoelectric coefficients, Capacitance and effective dielectric coefficient increased with the volume fraction of PZT. Also, the processing parameters such as spin-speed/time profiles and depositing techniques influenced the piezoelectric and dielectric properties of the dome-shaped devices. In particular, the piezoelectric strain coefficients in this work increased by a factor of 10 via use of the Corona polarization. Also, the piezoelectric strain coefficients of this work increased by a factor of 20 in comparison with our previous work in the design of dome-shaped 0–3 composite actuators. In addition, the dissipation factor associated with dielectric losses for this work decreased by nearly half. These results indicate that devices such as these may have potential for applications such as sensor, actuator, capacitor and low-power energy harvesting.

Declaration of Competing Interest

The authors declare that they have no known competing financial interests or personal relationships that could have appeared to influence the work reported in this paper.

Acknowledgements

This material is based upon work supported by the National Science Foundation under Grant Numbers: EEC1659818, EEC1263250 and EEC1407266. In addition, we would like to acknowledge support from the New Jersey Space Grant Consortium.

References

[1] Haertling GH. Ferroelectric ceramics: history and technology. J Am Ceram Soc 1999;82(4):797–818.
[2] Nisar A, Afzulpurkar N, Mahaisavariya B, Tuantranont A. MEMS-based micropumps in drug delivery and biomedical applications. Sens Actuators B Chem 2008;130(2):917–42.
[3] Buchanan RC, Park E, Surana R, Tennakone H, Tennakone K. High piezoelectric actuation response in graded Nd2O3 and ZrO2 doped BaTiO3 structures. J Electroceramics 2011;26(1–4):116–21.
[4] Choi S, Lee H, Moon W. A micro-machined piezoelectric hydrophone with hydrostatically balanced air backing. Sens Actuators A Phys 2010;158(1):60–71.
[5] Lee H, Choi S, Moon W. A micro-machined piezoelectric flexural-mode hydrophone with air backing: Benefit of air backing for enhancing sensitivitya). J Acoust Soc Am 2010;128(3):1033–44.
[6] Cook-Chennault K, Thambi N, Sastry A. Powering MEMS portable devices—a review of non-regenerative and regenerative power supply systems with special emphasis on piezoelectric energy harvesting systems. Smart Mater Struct 2008;17(4):43001.
[7] Cook-Chennault KA, Thambi N, Bitetto MA, Hameyie E. Piezoelectric energy harvesting a green and clean alternative for sustained power production. Bull Sci Technol Soc 2008;28(6):496–509.
[8] Amirouche F, Zhou Y, Johnson T. Current micropump technologies and their biomedical applications. Microsyst Technol 2009;15(5):647–66.
[9] Teymoori MM, Abbaspour-Sani E. Design and simulation of a novel electrostatic peristaltic micromachined pump for drug delivery applications. Sens Actuators A Phys 2005;117(2):222–9.
[10] Browe DP, et al. Characterization and optimization of actuating poly(ethylene glycol) diacrylate/acrylic acid hydrogels as artificial muscles. Polymer 2017;117(May):331–41. https://doi.org/10.1016/j.polymer.2017.04.044.
[11] McClarren B, Olabisi R. Strain and vibration in mesenchymal stem cells. Int J Biomater 2018. https://doi.org/10.1155/2018/8686794. Art no.8686794.
[12] Choi JP, Kim KS, Seo YH, Kim BH. Design and fabrication of synthetic air-jet micropump. Int J Precis Eng Manuf 2011;12(2):355–60.
[13] Harrison J, Ounaies Z. Piezoelectric polymers. Wiley Online Library; 2002.

[14] Dargahi J. Piezoelectric and pyroelectric transient signal analysis for detection of the temperature of a contact object for robotic tactile sensing. Sens Actuators A Phys 1998;71(1):89–97.
[15] Mossi KM, Selby GV, Bryant RG. Thin-layer composite unimorph ferroelectric driver and sensor properties. Mater Lett 1998;35(1):39–49.
[16] Peng J, Chao C, Tang H. Piezoelectric micromachined ultrasonic transducer based on dome-shaped piezoelectric single layer. Microsyst Technol 2010;16(10):1771–5.
[17] Man-Soon Y, Sung-Moo H, Soon-Chul U. A newly designed chopper for pyroelectric infrared sensor by using a dome-shaped piezoelectric linear motor (DSPLM). J Electroceramics 2009;23(2–4):242–7.
[18] Feng G-H. A piezoelectric dome-shaped-diaphragm transducer for microgenerator applications. Smart Mater Struct 2007;16(6):2636.
[19] Feng G-H, Kim ES. Piezoelectrically actuated dome-shaped diaphragm micropump. Microelectromech. Systems, J. 2005;14(2):192–9.
[20] Feng G-H, Sharp CC, Zhou Q, Pang W, Kim ES, Shung K. Fabrication of MEMS ZnO dome-shaped-diaphragm transducers for high-frequency ultrasonic imaging. J Micromech. Microengineering 2005;15(3):586.
[21] Cheng C, Tu S. Fabrication of a novel piezoelectric actuator with high load-bearing capability. Sens Actuators A Phys 2008;141(1):160–5.
[22] Banerjee S. An experimental and theoretical analysis of two and three phase epoxy based piezoelectric composites. Rutgers University-Graduate School-New Brunswick; 2013.
[23] Dietze M, Es-Souni M. Structural and functional properties of screen-printed PZT–PVDF-TrFE composites. Sens Actuators A Phys 2008;143(2):329–34.
[24] Arlt K, Wegener M. Piezoelectric PZT/PVDF-copolymer 0-3 composites: aspects on film preparation and electrical poling. Dielectrics and Electrical Insulation, IEEE Transactions on 2010;17(4):1178–84.
[25] van den Ende DA, Groen WA, van der Zwaag S. The effect of calcining temperature on the properties of 0-3 piezoelectric composites of PZT and a liquid crystalline thermosetting polymer. J Electroceramics 2011;27(1):13–9.
[26] Woo S-C, Park KH, Goo NS. Influences of dome height and stored elastic energy on the actuating performance of a plate-type piezoelectric composite actuator. Sens Actuators A Phys 2007;137(1):110–9.
[27] Ngernchuklin P, Akdogan E, Safari A, Jadidian B. Electromechanical displacement of piezoelectric-electrostrictive monolithic bilayer composites. J Appl Phys 2009;105(3):4102.
[28] Yoon KJ, Shin S, Park HC, Goo NS. Design and manufacture of a lightweight piezo-composite curved actuator. Smart Mater Struct 2002;11(1):163.
[29] Li C, Wu P-M, Lee S, Gorton A, Schulz MJ, Ahn CH. Flexible dome and bump shape piezoelectric tactile sensors using PVDF-TrFE copolymer. Microelectromech Systems, J 2008;17(2):334–41.
[30] Chen H, Fan C, Meng Z. Preparation and electromechanical properties of a piezoelectric ceramic dome-like actuator with d 31 gradients. Curr Appl Phys 2011;11(1):S324–7.
[31] Banerjee S, Du W, Wang L, Cook-Chennault KA. Fabrication of dome-shaped PZT-epoxy actuator using modified solvent and spin coating technique. J Electroceramics 2013;31(1–2 October):148–58. https://doi.org/10.1007/s10832-013-9834-8.
[32] Garcia FG, Soares BG, Pita V, Sanchez R, Rieumont J. Mechanical properties of epoxy networks based on DGEBA and aliphatic Amines," (in English). J Appl Polym Sci 2007;106(3 November):2047–55. https://doi.org/10.1002/app.24895.
[33] Durairaj R, Man LW. Effect of epoxy and filler concentrations on curing behaviour of isotropic conductive adhesives. J Therm Anal Calorim 2011;105(1 July):151–5. https://doi.org/10.1007/s10973-011-1340-0.
[34] McCoy JD, et al. Cure mechanisms of diglycidyl ether of bisphenol A (DGEBA) epoxy with diethanolamine. Polymer 2016;105:243–54. https://doi.org/10.1016/j.polymer.2016.10.028.
[35] Marincel DM, et al. Domain Wall Motion Across Various Grain Boundaries in Ferroelectric Thin Films. J Am Ceram Soc 2015;98(6 June):1848–57. https://doi.org/10.1111/jace.13535.
[36] Furukawa T, Fujino K, Fukada E. Electromechanical properties in the composites of epoxy resin and PZT ceramics. Jpn J Appl Phys 1976;15(11):2119–29.
[37] Furukawa T, Fujino K, Fukada E. Piezoelectric properties in the composite systems of polymers and PZT ceramics. J Appl Phys 1979;50(7):4904–12.
[38] Barthelmes G, Pratsinis SE, Buggisch H. Particle size distributions and viscosity of suspensions undergoing shear-induced coagulation and fragmentation. Chem Eng Sci 2003;58(13 July):2893–902. https://doi.org/10.1016/s0009-2509(03)00133-7.
[39] Seema A, Dayas KR, Varghese JM. PVDF-PZT-5H composites prepared by hot press and tape casting techniques. J Appl Polym Sci 2007;106(1 October):146–51. https://doi.org/10.1002/app.26673.
[40] Satish B, Sridevi K, Vijaya MS. Study of piezoelectric and dielectric properties of ferroelectric PZT-polymer composites prepared by hot-press technique. J Phys D-Appl Phys 2002;35(16 August):2048–50. https://doi.org/10.1088/0022-3727/35/16/321. Art no. Pii s0022-3727(02)35871-35876.
[41] Nhuapeng W, Tunkasiri T. Properties of 0-3 lead zirconate titanate-polymer composites prepared in a centrifuge. J Am Ceram Soc 2002;85(3 March):700–2 [Online]. Available: ://WOS:000174409800029.
[42] Liu XF, Xiong CX, Sun HJ, Dong LJ, Li R, Liu Y. Characterization of PZT/PVC composites added with carbon black," (in English). J Wuhan Univ Technol-Mat Sci Edit 2005;20(4 December):60–4 [Online]. Available: ://WOS:000234698000018.
[43] Venkatragavaraj E, Satish B, Vinod PR, Vijaya MS. Piezoelectric properties of ferroelectric PZT-polymer composites. J Phys D-Appl Phys 2001;34(4 Febuary):487–92. https://doi.org/10.1088/0022-3727/34/4/308.
[44] Sundar U, Cook-Chennault KA, Banerjee S, Refour E. Dielectric and piezoelectric properties of percolative three-phase piezoelectric polymer composites. J Vacuum Sci Technol B 2016;34(4 July):041232https://doi.org/10.1116/1.4955315.
[45] Cho SD, Lee JY, Paik KW. *Effects of particle size on dielectric constant and leakage current of epoxy/barium titanate (BaTiO3) composite films for embedded capacitors* (Advances in Electronic Materials and Packaging 2001). 2001. p. 63–8.
[46] Thamjaree W, Nhuapeng W, Chaipanich A, Tunkasiri T. Fabrication of combined 0-3 and 1-3 connectivities PZT/epoxy resin composites. in English), Appl. Phys. A-Mater. Sci. Process. 2005;81(7 November):1419–22. https://doi.org/10.1007/s00339-004-3136-6.
[47] Ben Ishai P, Talary MS, Caduff A, Levy E, Feldman Y. Electrode polarization in dielectric measurements: a review. Meas Sci Technol 2013;24(10 October):102001https://doi.org/10.1088/0957-0233/24/10/102001.